

Interaction-induced conducting-nonconducting transition of ultra-cold atoms in 1D optical lattices

Chih-Chun Chien¹, Daniel Gruss², Massimiliano Di Ventra³, and Michael Zwolak²

¹*Theoretical Division, Los Alamos National Laboratory, MS B213, Los Alamos, NM 87545, USA*

²*Department of Physics, Oregon State University, Corvallis, OR 97331, USA*

³*Department of Physics, University of California, San Diego, CA 92093, USA*

(Dated: November 20, 2012)

The study of time-dependent, many-body transport phenomena is increasingly within reach of ultra-cold atom experiments. We show that the introduction of spatially inhomogeneous interactions, e.g., generated by optically-controlled collisions, induce a conducting-to-nonconducting transition in the transport of atoms in 1D optical lattices. Specifically, we simulate the dynamics of interacting fermionic atoms via a micro-canonical transport formalism within both mean-field and other approximations. For weakly repulsive interactions, a quasi steady-state atomic current develops that is similar to the situation occurring for electronic systems subject to an external voltage bias. We also find that this atomic current is robust against the details of how the interaction is switched on. As the interactions exceed a threshold value, a mean-field conducting-to-nonconducting transition occurs due to energetic constraints. This transition is preceded by the atomic equivalent of negative differential conductivity observed in transport across solid-state structures, but here the eventual nonconducting state is one that emerges dynamically.

PACS numbers: 72.10.-d, 67.10.Jn, 03.75.Mn

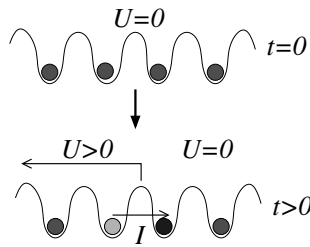


Figure 1. Schematic plot of the experimental set up we simulate: Non-interacting ultra-cold fermions are loaded into the lowest energy state of a 1D homogeneous optical lattice. At $t = 0$, a focused laser beam then induces on-site repulsive interactions of the Hubbard type on the left half of the lattice. Due to the imbalance of interactions in the middle, a mass current is induced. We emphasize that there is no need to “mechanically” set the atoms out of equilibrium by tilting a potential nor is it necessary to introduce additional species of atoms or dissipation. Moreover, this setup may also be implemented to study quench dynamics [13]. The gray dots emphasize that atoms may be in a superposition of different quantum states.

I. INTRODUCTION

Advances in experimental studies of quantum transport of ultra-cold atoms in optical lattices [1–4] draw attention to different aspects of non-equilibrium physics. In conventional condensed matter settings, an electrical current is induced by applying a voltage difference across the sample. The interactions of the charge carriers are usually homogeneous, except near impurities. In contrast, ultra-cold atoms are charge neutral and so far the motion of an atomic cloud has been generated by placing the cloud away from its equilibrium position [1] or by a sudden shift of the minimum of its trapping potential or its distortion [2–4]. The interactions are generated by either adding another species of atoms [1] or tuning magnetic-field controlled collisions [3, 4].

In this paper we instead suggest a method to drive a mass current of atoms via *local tuning of interactions*. This, in turn, reveals interesting phenomena otherwise difficult to observe in conventional solid state systems. A key to realize interaction-induced transport is controllable inhomogeneous interactions – a novel possibility offered by optically tunable collisions of ultra-cold atoms. The optical Feshbach resonance (OFR) [5–8] is a promising technique for controlling interactions *locally* using focused laser beams. For instance, the spatial modulation of density using the OFR of bosons [6] demonstrates the power of controllable inhomogeneous interactions. Other exotic equilibrium structures may also be generated by using this tool [9].

We also point out that these optically controlled interactions can be *time dependent* by turning on/off the induced interactions at certain times. The sudden imbalance of interactions within the cloud drives the system out of equilibrium. Thus, instead of using external driving mechanisms such as a voltage bias, it is possible, with suitable initial conditions and patterns of interactions, to induce a mass current. We show that for reasonably weak interactions the mass current of fermions is similar to a charge current in electronic systems. At a threshold interaction strength (dependent on the filling) a conducting-to-nonconducting transition occurs. This transition is due to a mismatch of energy spectra between the interacting and non-interacting parts of the system. Preceding the transition is a many-body counterpart of negative differential conductivity observed in solid-state structures [10, 11], where changes in the carrier density or subdivisions of Brillouin zones cause non-monotonic dependence of the current on the external field strength. Recently it has been shown that negative mobility of cold atoms could be demonstrated in temporally modulated optical lattices [12]. Here, instead we propose that one may observe negative differential conductance in a static optical lattice by tuning the interactions in real space.

II. INTERACTION-INDUCED TRANSPORT

In our approach – which explicitly follows the dynamics of mass transport – we implement the micro-canonical formalism (MCF) [14, 15] as in Ref. [16, 17] which monitors the evolution of the correlation matrix. When applied to a system of noninteracting atoms on a 1D optical lattice suddenly losing the atoms on the right half of the lattice, MCF shows very different dynamics for bosons and fermions [16]. While the bosonic current decays to zero in the thermodynamic limit, the fermionic current exhibits a quasi steady-state current corresponding to a plateau in the current as a function of time. Importantly, the MCF is designed for finite closed quantum systems so it is particularly suitable for studying the dynamics of ultra-cold atoms. Although our proposed setup can be applied to bosons, to explore their dynamics theoretically one has to consider also the effect of the quasi-condensate which renders the analysis more involved. Therefore, in this paper we focus only on fermions.

We consider $N_{p\sigma}$ ($\sigma = \uparrow, \downarrow$) two-component fermions, with $N_{p\uparrow} = N_{p\downarrow}$, loaded into a 1D optical lattice of size N , see Fig. 1. This type of finite-length 1D lattice may be generated by inserting a thin optical barrier [18] into a ring of optical lattice [19]. The resulting C-shaped lattice is geometrically identical to the setup here. This confining potential creates a uniform lattice and does not require a background harmonic trapping potential parallel to the lattice. The background interactions are assumed to

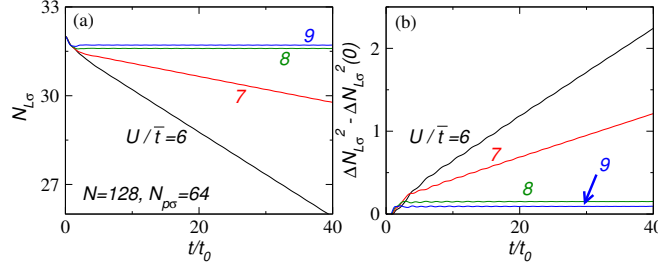


Figure 2. (Color online) (a) $N_{L\sigma}$ and (b) $\Delta N_{L\sigma}^2 - \Delta N_{L\sigma}^2(t=0)$ with $N = 128$ and $N_{p\sigma} = 64$ for each species from mean-field dynamics.

be negligible. The system is initially described by the tight-binding tunneling Hamiltonian $H_0 = -\tilde{t} \sum_{\langle ij \rangle, \sigma} c_{i\sigma}^\dagger c_{j\sigma}$, where $\langle ij \rangle$, \tilde{t} , $c_{i\sigma}^\dagger$ ($c_{i\sigma}$) denote nearest-neighbor pairs, the hopping coefficient, and the creation (annihilation) operator of site i , respectively. The unit of time is $t_0 \equiv \hbar/\tilde{t}$.

The initial state corresponds to the lowest energy state of H_0 , with no correlations between up and down spin states (see, e.g., Ref [16, 17]). The system is then set out of equilibrium by introducing interactions among atoms on the left half of the lattice by, e.g., optically-induced collisions using a focused laser beam. Here we concentrate on moderate repulsive interactions and non-integer filling. This allows us to focus on the dynamics induced by the interactions and avoid unnecessary confusions about possible equilibrium phase transitions such as the BCS instability or the Mott-insulating phase in uniform and static interacting systems [20]. We model an instantaneous switch-on of the interactions with a sharp interface between the interacting and non-interacting regions and relax the former condition later on.

The Hamiltonian generating the dynamics is

$$H_e = H_0 + \sum_{i \in L} U \hat{n}_{i\sigma} \hat{n}_{i\bar{\sigma}}. \quad (1)$$

Here $\hat{n}_{i\sigma} = c_{i\sigma}^\dagger c_{i\sigma}$, U is the onsite repulsive coupling constant, L denotes the left half of the lattice, and $\bar{\sigma}$ is the opposite of σ . This model should be appropriate for moderate lattice depth [21]. The equations of motion for the correlation matrix are $i(\partial \langle c_{i\sigma}^\dagger c_{j\sigma} \rangle / \partial t) = \langle [c_{i\sigma}^\dagger, H_e] c_{j\sigma} \rangle + \langle c_{i\sigma}^\dagger [c_{j\sigma}, H_e] \rangle$, where $[\cdot, \cdot]$ denotes the commutator of the corresponding operators. The explicit expression can be found using standard anti-commutation relations. After some algebra, one gets

$$i \frac{\partial \langle c_{i\sigma}^\dagger c_{j\sigma} \rangle}{\partial t} = \tilde{t} X_\sigma - U (\langle c_{i\bar{\sigma}}^\dagger c_{i\bar{\sigma}} c_{i\sigma}^\dagger c_{j\sigma} \rangle)_{i \in L} + U (\langle c_{i\sigma}^\dagger c_{j\sigma} c_{j\bar{\sigma}}^\dagger c_{i\bar{\sigma}} \rangle)_{j \in L}. \quad (2)$$

Here $X_\sigma \equiv \langle c_{i+1,\sigma}^\dagger c_{j\sigma} \rangle + \langle c_{i-1,\sigma}^\dagger c_{j\sigma} \rangle - \langle c_{i\sigma}^\dagger c_{j+1,\sigma} \rangle - \langle c_{i\sigma}^\dagger c_{j-1,\sigma} \rangle$. $n_i = \langle \hat{n}_i \rangle$ and $n_{i\sigma} = \langle \hat{n}_{i\sigma} \rangle$. We solve Eq. (2) both at the mean-field level and by adding higher-order correlations.

The mean-field level solution can be obtained by Wick decomposition of $\langle c_{i\bar{\sigma}}^\dagger c_{i\bar{\sigma}} c_{i\sigma}^\dagger c_{j\sigma} \rangle$ as $\langle c_{i\bar{\sigma}}^\dagger c_{i\bar{\sigma}} \rangle \langle c_{i\sigma}^\dagger c_{j\sigma} \rangle$ since no spin-flip mechanisms are present. This is the standard Hartree-Fock approximation. The equations are closed after this approximation. Thus the dynamics after the interaction is switched on can be monitored by integrating Eq. (2) with the initial condition $c_{ij\sigma}(t=0)$ given by the lowest energy state of the non-interacting Hamiltonian. We update Eq. (2) in a symmetric fashion so that $\langle c_{i\sigma}^\dagger c_{j\sigma} \rangle = \langle c_{i\bar{\sigma}}^\dagger c_{j\bar{\sigma}} \rangle$ at any time.

In addition to the current $I_\sigma = 2\tilde{t} \text{Im} \langle c_{N/2,\sigma}^\dagger c_{N/2+1,\sigma} \rangle$, we also evaluate the particle number on the left half lattice, $N_{L\sigma} = \langle \hat{N}_{L\sigma} \rangle$ and its fluctuations $\Delta N_{L\sigma}^2 = \langle \hat{N}_{L\sigma}^2 \rangle - \langle \hat{N}_{L\sigma} \rangle^2$, which is another property that can be determined experimentally. Here $\hat{N}_{L\sigma} = \sum_{i \in L} \hat{n}_{i\sigma}$. Explicitly,

$$\Delta N_{L\sigma}^2 = \sum_{i=1}^{N/2} n_{i\sigma} (1 - n_{i\sigma}) - 2 \sum_{i < j}^{N/2} |c_{ij\sigma}|^2. \quad (3)$$

Right before the interactions are switched on, there can be initial number fluctuations due to the wave nature of the initial quantum state. We thus present $\Delta N_{L(\sigma)}^2 - \Delta N_{L(\sigma)}^2(t=0)$ which reflects the change of the number fluctuations due to the interaction-induced dynamics.

III. RESULTS AND DISCUSSIONS

Figure 2 shows the particle number and its fluctuations of the left half lattice with $N = 128$ and $N_{p\sigma} = 64$ for each species. As U/\tilde{t} increases, one can see that instead of inducing more fermions to move from the left to the right, above a certain threshold

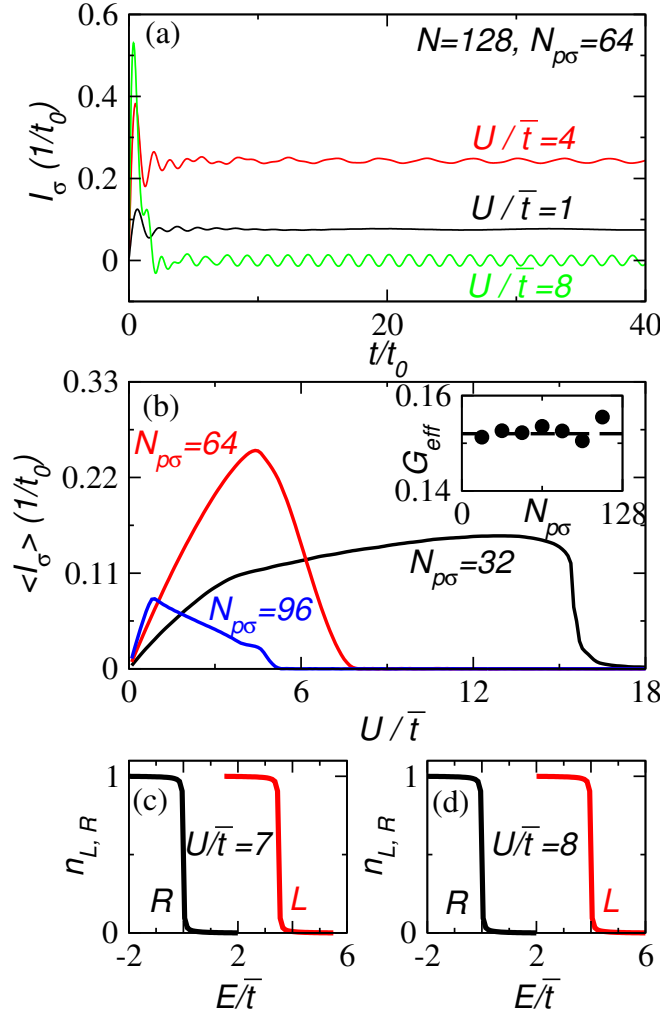


Figure 3. (Color online) (a) I_σ and (b) $\langle I_\sigma \rangle$ of the fermionic case with $N = 128$ and $N_{p\sigma} = 64$ for each species from mean-field dynamics. The inset of (b) shows $G_{eff} \equiv f^{-1} d\langle I_\sigma \rangle / dU$ (in units of $2\pi/h$) for small U/\bar{t} as a function of $N_{p\sigma}$ for $N = 128$, where $f = N_{p\sigma}/N$ is the initial filling factor. The dashed line shows $G_0 \approx 0.152$ in this unit. The energy spectra of the left (L) and right (R) half lattices when U is switched on are shown for $U/\bar{t} = 7$ (c) and $U/\bar{t} = 8$ (d). Here $N = 128$ and $N_{p\sigma} = 64$.

value the transport is no longer observed within a reasonable time scale (e.g., $t \leq (N/2)t_0$). This corresponds to a conducting-nonconducting transition and it can be found at other ratios of $f \equiv N_p/N$. In general the threshold U_c/\bar{t} decreases as f increases. We will show that this is because for higher filling the onsite interaction energy dominates more easily. One can see this transition even better in the average current itself.

We note that it has been shown that with suitable initial conditions non-interacting fermions can develop a quasi steady-state current (QSSC) [16, 22]. This is so also for the present interacting case. The fermionic current is shown in Figure 3(a) for $N = 128$ and $N_{p\sigma} = 64$ for each species. The plateaus shown in $I_\sigma(t)$ indicate the existence of QSSCs. To smooth over small oscillations, we define an averaged current as $\langle I_\sigma \rangle \equiv (1/30t_0) \int_{10t_0}^{40t_0} dt I_\sigma(t)$ and plot $\langle I_\sigma \rangle$ as a function of U/\bar{t} for $N_{p\sigma} = 32, 64, 96$ in Fig. 3(b). For small U/\bar{t} we clearly see that the averaged current increases linearly with U/\bar{t} . Then the dependence deviates from a linear form before the conducting-nonconducting transition. For even larger U/\bar{t} , $\langle I_\sigma \rangle$ decreases until no finite averaged current can be found. The non-monotonic dependence of $\langle I_\sigma \rangle$ on U resembles the negative differential conductivity observed in conventional solid-state devices [10, 11].

The interaction term thus acts as a bias on the left half lattice if U/\bar{t} is small. Here we investigate the validity of this statement. By extracting the slope of the linear part of $\langle I_\sigma \rangle$ for small U/\bar{t} , one can study how efficient the interaction can induce a current. The inset of Fig. 3(b) shows the effective conductance $G_{eff} \equiv f^{-1} d\langle I_\sigma \rangle / dU$ as a function of $N_{p\sigma}$ for a fixed N , where $f = N_{p\sigma}/N$ is the initial filling factor. As $N_{p\sigma} \rightarrow N$ the system approaches a band insulator [23] and there is only a tiny range of U/\bar{t} where a finite $\langle I_\sigma \rangle$ exists. This could contribute to some inaccuracy of the extraction of the slope close to $N_{p\sigma} \rightarrow N$. Nevertheless, as shown on the inset of Fig. 3(b) the effective conductance is close to the ideal quantized conductance

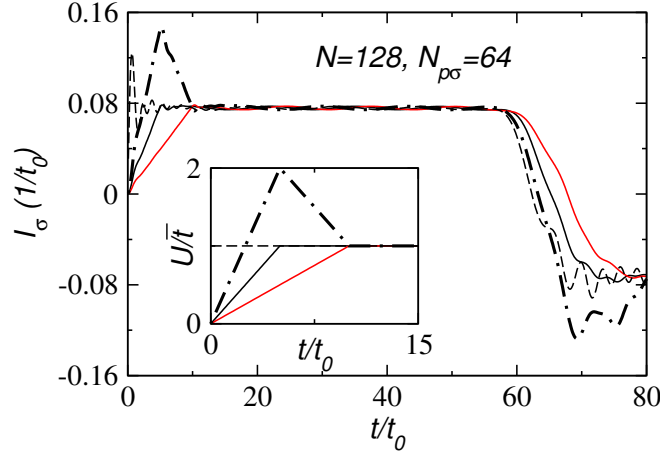


Figure 4. (Color online) Currents induced by different ways of switching-on the interaction from mean-field dynamics: A sudden switch-on of the interaction (dashed line), linear switch-ons with switching times $t_m = 5t_0$ (black) and $t_m = 10t_0$ (red), and a multi-step switch-on (dot-dash line). The inset shows the time dependence of U for the four cases. Here $N = 128$ and $N_{p\sigma} = 64$.

$G_0 = (2\pi\hbar)^{-1}$ for arbitrary initial filling. This establishes the feasibility of using a weak inhomogeneous interaction as an efficient driving force for inducing a current and its correspondence with a bias, $\Delta\mu = fU$.

In the weak interaction regime, we found another interesting phenomenon. By considering different ways of switching on the interaction, one may wonder whether the system will reach the same magnitude of the QSSC. We simulate different switching-on scenarios by introducing a time scale t_m such that the interaction grows from zero to its full value during t_m and remains a constant after that. Figure 4 shows that despite different time-dependences of the interaction, the system always reaches the same magnitude of the QSSC. We have also checked other more complicated functional forms for switching on the interaction and found the same QSSC. Importantly, even if the system is over-excited by a spike in the time dependence of U , when U comes back to a constant value the height of the QSSC coincides with the case of a sudden switch-on of the interaction as shown on Fig. 4. Thus the magnitude of the QSSC is robust (memory-less) against different ways the interaction is switched on. This feature makes the interaction-induced transport appealing for atomtronics since a steady output (the QSSC) is insensitive to the transient behavior of the driving force (the interaction).

When the optically-induced interactions are switched on, it is possible that the onsite potential could be shifted due to the increase of the kinetic energy of the atoms interacting with the incoming photons. We study possible effects by adding an extra term $V \sum_{i \in L, \sigma} \hat{n}_{i\sigma}$ to H_e of Eq. (1) to simulate this effect with a positive V . This shift of the onsite potential acts like a bias so one might expect that more current will flow to the other side. However, the conducting-nonconducting transition is robust against this positive potential shift. The energetic mechanism described below will make it clear why a positive potential shift will not remove the transition, thus showing that it is not sensitive to this type of modification of the Hamiltonian.

We now discuss the reason behind the transition, which is energetic in nature. In order to obtain a “macroscopic” steady-state current, αN particles must be transferred from the left to the right halves, where α is some small proportionality constant. However, this entails a change in energy, as the particle density decreases on the site with interactions, and this effect must be compensated by an energy change due to rearrangement of the single particle states. To be more concrete, immediately after interactions are turned on, the system is still in the ground state of H_0 . However, the energy has shifted to

$$E = E_0 + U \sum_{i \in L} \langle n_{i\sigma} n_{i\bar{\sigma}} \rangle_0 = E_0 + U \sum_{i \in L} \langle n_{i\sigma} \rangle_0 \langle n_{i\bar{\sigma}} \rangle_0, \quad (4)$$

where Wick’s theorem has been applied since the system is in the ground state of H_0 . The subscript of $\langle \dots \rangle$ denotes the time when the expectation is taken. For half-filling, this gives an energy $E = E_0 + UN/8$. For arbitrary filling f , it is

$$E \approx E_0 + f^2 UN/2, \quad (5)$$

where the expression is approximate since not all site occupation numbers will be exactly f (for each spin component).

The energy at some later time will still be E (since no further changes have been made to the Hamiltonian), but will have the form

$$E = \langle H_0 \rangle_t + U \sum_{i \in L} \langle n_{i\sigma} \rangle_t \langle n_{i\bar{\sigma}} \rangle_t \quad (6)$$

in the mean-field approximation. Assuming the αN atoms are taken uniformly from the left half, the energy is

$$E \approx \langle H_0 \rangle_t + f^2 UN/2 - \alpha f UN. \quad (7)$$

Taking the difference of Eq. (7) and Eq. (5), and using energy conservation, gives $\langle H_0 \rangle_t - E_0 \approx \alpha f UN$. However, the quantity $\langle H_0 \rangle_t - E_0$ can not be arbitrary, since we have a finite bandwidth. Regardless of whether one has an interacting or noninteracting state, the largest energy change due to the H_0 contribution is $4\tilde{t}\alpha N$, corresponding to taking the αN particles from the lowest part of the band (on the left half) to the highest part (on the right half). This gives

$$\alpha f UN \lesssim 4\tilde{t}\alpha N \longrightarrow U \lesssim 4\tilde{t}/f \quad (8)$$

and thus results in a threshold value of U . Beyond this value of U , a macroscopic current can not flow. We remark that here we consider the lowest energy band of the optical lattice. If the interaction energy exceeds the band gap separating different bands, the system may re-enter a conducting state.

To demonstrate this energetic mechanism, Fig. 3(c) and (d) show the energy spectra of the left (L) and right (R) half lattices when U is switched on for $N = 128$ with $N_{p\sigma} = 64$. When $U/\tilde{t} = 7$ (panel (c)), there is still an overlap between the two spectra and exchanging atoms in an energy-conserving fashion is possible. For $U/\tilde{t} = 8$ (panel (d)), there is no overlap between the two spectra and the system evolves into a nonconducting state. This theory also explains why the nonconducting state is robust against an additional positive onsite bias. Any further increase of the onsite energy separates the two energy spectra of the left and the right sides even farther so the nonconducting state remains. Importantly, this energetic mechanism applies to other types of setups for studying transport phenomena. For example, by introducing a step-function bias to the lattice potential and tuning the bias, there is also a conducting-nonconducting transition of the same nature (see Appendix A).

We note, however, that other possibilities may occur in interacting systems for large U/\tilde{t} when a homogeneous conducting state is no longer favorable. From Eq. (6), states could be generated that have an oscillating density which would give enough “energetic relief” to allow a macroscopic current to flow [24]. In the mean-field solution, however, the state of the system is steered into a nonconducting state that is a *dynamically generated zero current state*. Since the conducting-nonconducting transition emerges dynamically, it should not be confused with conventional transitions of equilibrium states. For example, there are several differences when the dynamically-generated nonconducting state is compared to the Mott insulating state in equilibrium [20]: *i*) the nonconducting state could occur at arbitrary filling while the Mott insulator needs integer filling; *ii*) the mechanism behind the nonconducting state is energy conservation while that behind the Mott insulator is the minimization of ground state energy; *iii*) the nonconducting state depends on its initial state and evolution, while the Mott state is the ground state of the corresponding Hamiltonian.

IV. HIGHER-ORDER CORRELATIONS

We finally check whether the conducting-nonconducting transition survives when higher-order correlation functions (beyond using the Wick decomposition) are considered. The equations of motion of two-particle correlation functions were preserved and the three-particle correlation functions were decomposed into two- and single-particle functions as shown below. Importantly, we found that the conducting-nonconducting transition is still observable. We thus emphasize that even with the inclusion of higher-order corrections, the system dynamically evolves into the nonconducting state, thus supporting that this energetically driven transition should be observable experimentally [25].

To monitor the dynamics, we integrate the equations of motion while respecting the symmetry between the two spin indices. The equations of motion of the correlation matrix elements (or single-particle correlation functions) now include two-particle correlation functions. Above, we closed the set of equations using the Wick decomposition to write two-particle correlations as products of single-particle correlation functions, which is the Hartree-Fock (or mean-field) approximation. We now consider the case where the three-particle correlation functions are decomposed into products of single-particle correlation functions and two-particle correlation functions, e.g.,

$$\begin{aligned} \langle c_{i\sigma}^\dagger c_{j\sigma} c_{k\sigma}^\dagger c_{l\sigma} c_{m\bar{\sigma}}^\dagger c_{n\bar{\sigma}} \rangle = & \frac{1}{3} \left(\langle c_{m\bar{\sigma}}^\dagger c_{n\bar{\sigma}} \rangle \langle c_{i\sigma}^\dagger c_{j\sigma} c_{k\sigma}^\dagger c_{l\sigma} \rangle \right. \\ & + \langle c_{i\sigma}^\dagger c_{j\sigma} \rangle \langle c_{m\bar{\sigma}}^\dagger c_{n\bar{\sigma}} c_{k\sigma}^\dagger c_{l\sigma} \rangle - \langle c_{i\sigma}^\dagger c_{l\sigma} \rangle \langle c_{k\sigma}^\dagger c_{j\sigma} c_{m\bar{\sigma}}^\dagger c_{n\bar{\sigma}} \rangle + \delta_{jk} \langle c_{i\sigma}^\dagger c_{l\sigma} \rangle \langle c_{m\bar{\sigma}}^\dagger c_{n\bar{\sigma}} \rangle \\ & \left. - \langle c_{k\sigma}^\dagger c_{j\sigma} \rangle \langle c_{i\sigma}^\dagger c_{l\sigma} c_{m\bar{\sigma}}^\dagger c_{n\bar{\sigma}} \rangle + \langle c_{k\sigma}^\dagger c_{l\sigma} \rangle \langle c_{i\sigma}^\dagger c_{j\sigma} c_{m\bar{\sigma}}^\dagger c_{n\bar{\sigma}} \rangle + \delta_{jk} \langle c_{i\sigma}^\dagger c_{l\sigma} c_{m\bar{\sigma}}^\dagger c_{n\bar{\sigma}} \rangle \right). \quad (9) \end{aligned}$$

This allows us to include all of the two-particle correlation functions in the simulation. Since there are three ways to decompose the three-particle correlation functions, we chose to average the contributions of each in order to reduce the numerical instability of the simulation.

We have computed the currents by solving the mean-field equations of motion and the equations that include two-particle correlations for $N = 40$ and $N_{p\sigma} = 20$. The results are shown in Figure 5 and they agree qualitatively. More importantly, while

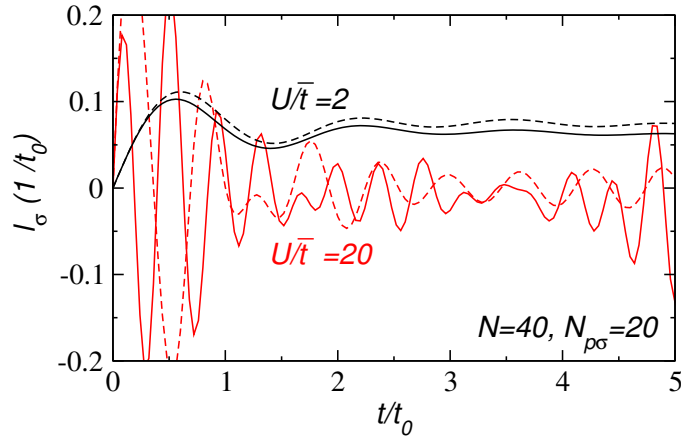


Figure 5. (Color online) The currents from the mean-field approximation (dashed lines) and from the simulations including two-particle correlations (solid lines). Black (red) lines correspond to $U/\bar{t} = 2$ (20). Here $N = 40$ and $N_{p\sigma} = 20$.

finite smooth currents are found in both approaches for small U/\bar{t} , the current oscillates rapidly with a small amplitude around zero for large U/\bar{t} . Figure 6 shows the average current including higher-order calculations, and is similar to the mean field case in Figure 3(b): There is an increase then a decrease in $\langle I_\sigma \rangle$ as U/\bar{t} is increased, which is also observed for other higher order approximations. There are differences, however, with the mean field results, as shown in Figure 7, especially within the center of the lattice. Nevertheless, there is no indication that a conducting state emerges for large U (e.g., a state with density oscillations sufficient to counter balance the energetic constraints discussed above).

We note that inclusion of the two-particle correlations is only a short time approximation and the simulations can become unstable for intermediate to long times. We have thus restricted these simulations to short times and are therefore limited to averaging over shorter time scales than above. This means that the averaging partially truncates oscillations and the effect of this partial truncation is to give a finite value to $\langle I_\sigma \rangle$ even when a longer average would give zero. This will be more prominent for shorter averages, i.e., in the absence of transient effects, one expects that the boundary will give a residual contribution of $\langle I_\sigma \rangle \propto 1/U$, as U gives the frequency scale of oscillations (for large U). The current versus time shows that this is indeed what is happening: There are faster oscillations as U is increased (and also as f is increased). When averaging to get $\langle I_\sigma \rangle$, one will not obtain zero for large U but rather some residual effect because of the short time average. The inset of Figure 6 shows this tail. For the filling greater than $1/2$, the average current is consistent with this interpretation, and thus the nonconducting state is forming. For filling equal to $1/2$, the results are ambiguous, as the oscillations are both slower than the higher filling cases and many-body correlations are more important. Nevertheless, for $f = 1/2$, the average current still decays to zero, which is indicative of the nonconducting state.

Furthermore, our results suggest that for small U/\bar{t} the transient time to reach a quasi steady state is only a few t_0 while the duration of the QSSC can extend much further than that. Thus for reasonably large lattices, the observation of an interaction-induced QSSC and the conducting-nonconducting transition is feasible.

V. CONCLUSION

In summary, we have shown that one may use time-dependent inhomogeneous interactions of ultra-cold atoms to explore non-equilibrium physics not easily realizable in conventional solid-state setups. In particular, we find a conducting-nonconducting transition, where the nonconducting state emerges dynamically. Importantly, the current in the weakly-interacting regime is robust against possible transient behavior of the driving force. Our micro-canonical simulations may be compared with other numerical methods such as the time-dependent density-matrix renormalization-group method [26] to further investigate the correlation effects. Our work not only sheds light on fundamental physics out of equilibrium, it may also lead to different designs of devices in the thriving field of atomtronics [27].

CCC acknowledges the support of the U. S. DOE through the LANL/LDRD Program. MD acknowledges support from the DOE grant DE-FG02-05ER46204 and UC Laboratories.

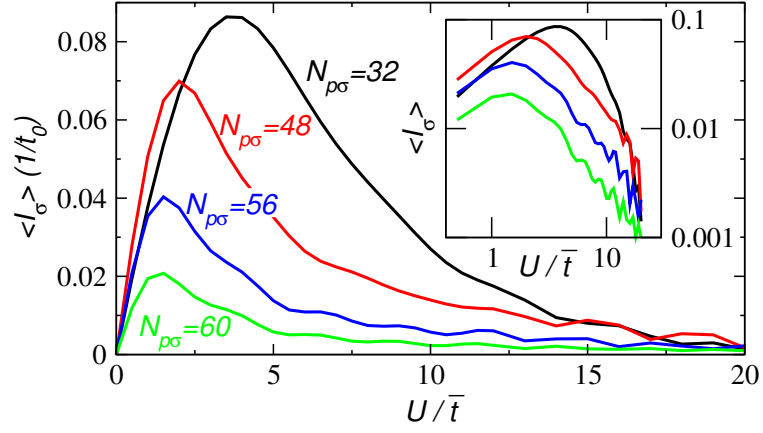


Figure 6. (Color online) $\langle I_\sigma \rangle$ of the fermionic case with $N = 64$ and $N_{p\sigma} = 32, 48, 56, 60$ from the simulations with two-particle correlations. Similar to Figure 3, the average current initially increases with U and then decreases. Here, the averaged current is computed from $t = 0$ to $t = 2.5t_0$. The inset of the plot shows the average current plotted on a log scale, which shows that it does indeed vary as $1/U^\alpha$ where α tends towards 1 as the filling increases ($\alpha \approx 2.95, 1.59, 1.43, 1.29$ for $N_{p\sigma} = 32, 48, 56, 60$ respectively). Partially truncated oscillations are thus likely responsible for the residual value of $\langle I_\sigma \rangle$ at large U .

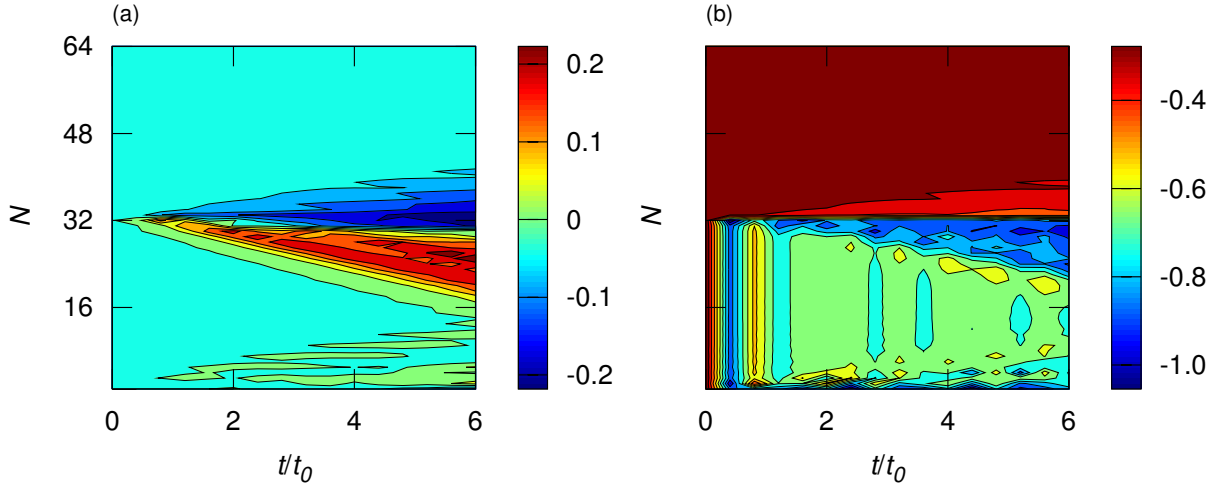


Figure 7. (Color online) (a) Difference between the onsite correlations $\langle \hat{n}_{i\sigma} \rangle$ as calculated using the mean field approximation and using the two-particle correlations and (b) the relative difference between the onsite density-density correlations $\langle \hat{n}_{i\sigma} \hat{n}_{i\bar{\sigma}} \rangle$. While the two approximations can differ in the value of these correlations, there is no evidence that density oscillations (beyond those seen in the mean field) emerge from the simulations. Thus, the formation of the nonconducting state for large U is expected.

Appendix A: Comparison of bias vs. interaction

When a bias is applied to a single-species noninteracting fermions in a uniform 1D lattice, the Hamiltonian is $H_B = -\tilde{t} \sum_{\langle ij \rangle} c_i^\dagger c_j + \frac{\mu_B}{2} \sum_{i \in L} c_i^\dagger c_i - \frac{\mu_B}{2} \sum_{i \in R} c_i^\dagger c_i$. We assume the initial state is the ground state of the Hamiltonian with zero bias ($\mu_B = 0$) and then it evolves according to H_B . For $N = 128$, we define $\langle I_\sigma \rangle = (1/30t_0) \int_{10t_0}^{40t_0} dt I_\sigma(t)$, where $t_0 \equiv \hbar/\tilde{t}$. Figure 8 (a) shows $\langle I_\sigma \rangle$ as a function of μ_B . One can see that above $\mu_B/\tilde{t} = 4$ no finite averaged current can be found. There is a conducting-nonconducting transition and the upper limit is independent of N_p/N , which can be seen by a similar analysis to Eqs. (4)-(8) in the main text.

As with the interaction case, energy conservation prohibits particles on the left with energy higher than the highest energy level of the right from entering the right half of the lattice. This occurs when μ_B is larger than the bandwidth of the original uniform lattice, which is $4\tilde{t}$. The particle distributions of the two half lattices when the interaction is switched on can be found as follows. The initial correlation matrix $c_{ij}(t=0)$ of the whole lattice is $\sum_{p=1}^{N_p} U_0^\dagger(i,p)U_0(p,j)$, where U_0 is the unitary matrix that diagonalizes the hopping Hamiltonian. After finding U_L and U_R that diagonalize the Hamiltonian of the left and the right half lattices with eigenvalues E_L and E_R , the particle distributions are given by $n_{L/R}(k) = \sum_{i,j \in L/R} (U_{L/R}^\dagger)_{kj} U_{ik} c_{ij}(t=0)$,

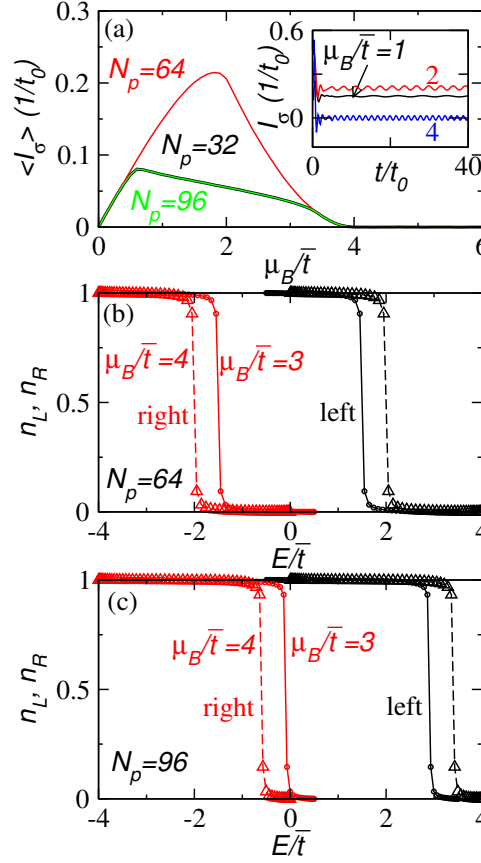


Figure 8. (a) $\langle I_\sigma \rangle$ as a function of μ_B for $N = 128$ and $N_p = 32, 64, 96$. The curves for $N_p = 32, 96$ coincide due to the particle-hole symmetry. Inset: The currents for $\mu_B/\bar{t} = 1, 2, 4$ (labeled next to each curve) with $N_p = 64$. (b) Particle distributions of the left half (black) and the right half (red) for $\mu_B/\bar{t} = 3$ (solid line) and 4 (dashed lines). The symbols show energy levels. Here $N = 128$ and $N_p = 64$. (c) Same as (b) but with $N_p = 96$.

where $k = 1, \dots, N/2$ labels the energy levels $E_{L/R}(k)$. Fig. 8 (b) and (c) show the particle distributions for the left and right half lattices for $\mu_B/\bar{t} = 3$ and 4 with $N_p = 64$ and 96. One can see that when the bottom of the left half energy band moves above the top of the band of the right, no current is expected since energy is conserved.

Taking the same definition for $\langle I_\sigma \rangle$ for the interaction-induced case, we plot $\langle I_\sigma \rangle$ as a function of U in Fig. 9. There is also a conducting-nonconducting transition, but the threshold value depends on the filling $N_{p\sigma}/N$. The left half lattice has Hamiltonian $H_L = \sum_{\langle ij \rangle \in L, \sigma} c_{i\sigma}^\dagger c_{j\sigma} + U \sum_{i \in L} \hat{n}_{i\sigma} \hat{n}_{i\bar{\sigma}}$. Here $\hat{n}_i = c_{i\sigma}^\dagger c_{i\sigma}$. To find the energy levels of H_L at $t = 0$, we replace $\hat{n}_{i\bar{\sigma}}$ by its expectation value, which is known from $c_{ij, \sigma}(t = 0)$ and we assume the particle number of the two species are equal. After diagonalizing $H_L^{eff} = \sum_{\langle ij \rangle \in L, \sigma} c_{i\sigma}^\dagger c_{j\sigma} + U \sum_{i \in L} n_{i\bar{\sigma}} \hat{n}_{i\sigma}$, we found $E_L(k)$ with $k = 1, \dots, k$ and the unitary matrix U_L . The right half lattice remains noninteracting and one can find $E_R(k)$ and U_R . The distribution functions are then given by $n_{L/R}(k) = \sum_{i,j \in L/R} (U_{L/R}^\dagger)_{kj} U_{ik} c_{ij}(t = 0)$.

Fig. 9 (b) and (c) show the distributions of the right and left half lattices for $N_{p\sigma} = 64$ and 96 and $N = 128$. The nonconducting states emerge slightly above $U/\bar{t} = 7$ ($U/\bar{t} = 5$) for $N_{p\sigma} = 64$ ($N_{p\sigma} = 96$). The distributions for U/\bar{t} below the threshold value still show observable overlaps between the filled states of the left half lattice and the empty states of the right half lattice. When U/\bar{t} is above the threshold value, the distributions of the two half lattices are separated so energy conservation forbids transport. We thus observe nonconducting states in both bias-induced and interaction-induced transport due to energy-level mismatches of the two half lattices. In the interacting case, however, there may exist states that could carry a current, but our simulations show that the nonconducting state emerges dynamically in the setup we examine.

-
- [1] H. Ott, E. de Mirandes, F. Ferlaino, G. Roati, G. Modugno, and M. Inguscio, Phys. Rev. Lett., **92**, 160601 (2004).
 [2] C. D. Fertig, K. M. O'Hara, J. H. Huckans, S. L. Rolston, W. D. Phillips, and J. V. Porto, Phys. Rev. Lett., **94**, 120403 (2005).

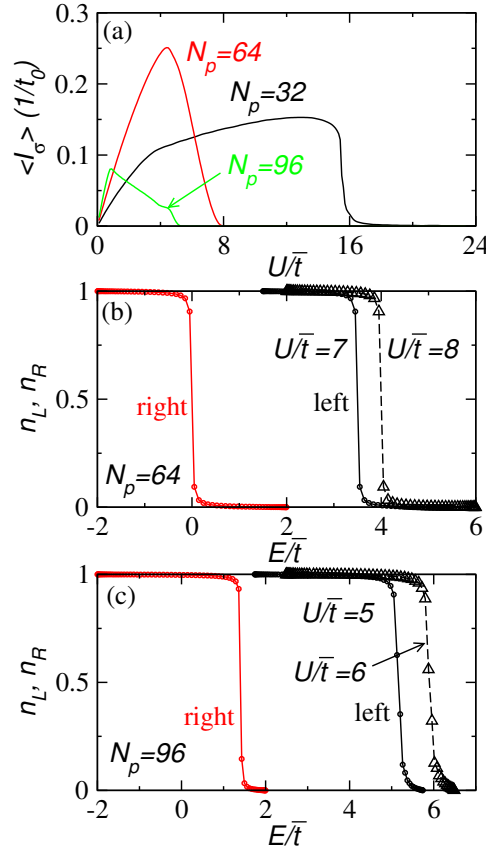


Figure 9. (a) $\langle I \rangle$ as a function of U for $N = 128$ and $N_p = 32, 64, 96$ from the mean-field approximation. (b) Particle distributions of the left half (black) and the right half (red) for $U/\bar{t} = 7$ (solid line) and 8 (dashed line). The symbols show energy levels. Here $N = 128$ and $N_{p\sigma} = 64$. (c) Same as (b) but $N_{p\sigma} = 96$ and $U/\bar{t} = 5$ (solid line) and 6 (dashed line).

- [3] N. Strohmaier, Y. Takasu, K. Gunter, R. Jordens, M. Kohl, H. Moritz, and T. Esslinger, Phys. Rev. Lett., **99**, 220601 (2007).
- [4] U. Schneider, L. Hackermuller, J. P. Ronzheimer, S. Will, S. Braun, T. Best, I. Bloch, E. Demler, S. Mandt, D. Rasch, and A. Rosch, Nat. Phys., **8**, 213 (2012).
- [5] T. Fukuhara, S. Sugawa, Y. Takasu, and Y. Takahashi, Phys. Rev. A, **79**, 021601 (2009).
- [6] R. Yamazaki, S. Taie, S. Sugawa, and Y. Takahashi, Phys. Rev. Lett., **105**, 050405 (2010).
- [7] S. Blatt, T. L. Nicholson, B. J. Bloom, J. R. Williams, J. W. Thomsen, P. S. Julienne, and J. Ye, Phys. Rev. Lett., **107**, 073202 (2011).
- [8] H. Wu and J. E. Thomas, Phys. Rev. Lett., **108**, 010401 (2012).
- [9] C. C. Chien, Phys. Lett. A, **376**, 729 (2012).
- [10] L. Esaki and R. Tsu, IBM J. Res. Develop., **14**, 61 (1970).
- [11] E. M. Conwell, Phys. Today, **23**, 35 (1970).
- [12] T. Salger, S. Kling, S. Denisov, A. Ponomarev, P. Hanggi, and M. Weitz, (2012), eprint, arXiv: 1202.5174.
- [13] A. Polkovnikov, K. Sengupta, A. Silva, and M. Vengalattore, Rev. Mod. Phys., **83**, 863 (2011).
- [14] M. Di Ventra and T. Todorov, J. Phys. Cond Matt., **16**, 8025 (2004).
- [15] M. Di Ventra, *Electrical Transport in Nanoscale Systems* (Cambridge University Press, 2008).
- [16] C. C. Chien, M. Zwolak, and M. Di Ventra, Phys. Rev. A, **85**, 041601(R) (2012).
- [17] C. C. Chien and M. Di Ventra, EPL, **99**, 40003 (2012).
- [18] A. Ramanathan, K. C. Wright, S. R. Muniz, M. Zelan, W. T. Hill III, C. J. Lobb, K. Helmerson, W. D. Phillips, and G. K. Campbell, Phys. Rev. Lett., **106**, 130401 (2011).
- [19] K. Henderson, C. Ryu, C. MacCormic, and M. G. Boshier, New J. Phys., **11**, 043030 (2009).
- [20] C. J. Pethick and H. Smith, *Bose-Einstein Condensation in Dilute Gases*, 2nd ed. (Cambridge University Press, 2008).
- [21] W. Hofstadter, J. I. Cirac, P. Zoller, E. Demler, and M. D. Lukin, Phys. Rev. Lett., **89**, 220407 (2002).
- [22] N. Bushong, N. Sai, and M. Di Ventra, Nano Lett., **5**, 2569 (2005).
- [23] For a single-band model of fermions considered here, $N_{p\sigma}/N = 1$ corresponds to a band insulator and no current can flow even in the presence of inhomogeneous interactions.
- [24] We found density modulations in the *nonconducting* state, too.
- [25] We cannot, however, exclude that the left-half (interacting) part may evolve into a density-modulating state or even a spin-density-wave state if the symmetry between spins is lifted.

- [26] F. Heidrich-Meisner, S. R. Manmana, M. Rigol, A. Muramatsu, A. E. Feiguin, and E. Dagotto, Phys. Rev. A, **80**, 041603(R) (2009).
- [27] R. A. Pepino, J. Cooper, D. Z. Anderson, and M. J. Holland, Phys. Rev. Lett., **103**, 140405 (2009).